Research Article

Raspberry-like gold-decorated silica (SS_x–AMPS–Au) nanoparticles for the reductive discoloration of dyes

Angelique Blanckenberg[1] · **Rehana Malgas-Enus**[1]

Abstract

SS_x–AMPS–Au nanoparticles were designed and synthesized for use as catalysts in the reductive discoloration of organic dyes. The catalysts are raspberry-like structures consisting of amorphous silica nanoparticle cores, SS_x (x = 20, 50 and 100 nm), functionalized with amine groups and decorated with discrete gold nanoparticles. Evaluation of these nano-raspberries for the discoloration of methylene blue in both metal-catalyzed and metal-mediated reactions showed significantly enhanced rates of reduction (< 900 s) as compared to the catalyst-free reactions (> 24 h). Furthermore, the SS_x–AMPS–Au nano-raspberries could also successfully reduce a range of anionic and cationic organic dyes, including methyl orange, rhodamine B, congo red, malachite green and crystal violet. The most promising catalyst was SS_{50}–AMPS–Au, which comprized of ~ 3.5 nm gold nanoparticles on a 50 nm silica sphere. SS_{50}–AMPS–Au showed significantly higher activity for all reactions. Comparison of the non-recyclable catalytic system and the recyclable metal-mediated system showed that the catalytic system is the greener of the two.

Graphic abstract

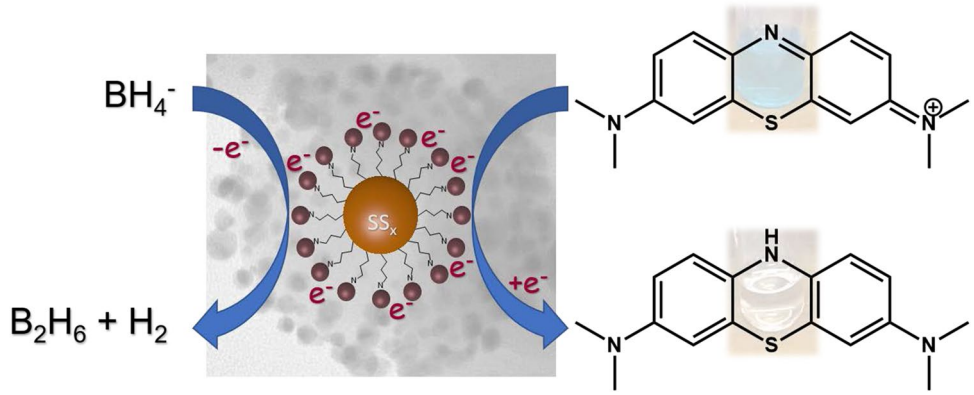

Keywords Nanocatalyst · Gold-decorated nanoparticles · Silica nanospheres · Raspberry-like structures · Dye discoloration

Electronic supplementary material The online version of this article (https://doi.org/10.1007/s42452-019-0821-9) contains supplementary material, which is available to authorized users.

✉ Rehana Malgas-Enus, rehana@sun.ac.za | [1]Department of Chemistry and Polymer Science, University of Stellenbosch, Private Bag X1, Matieland 7602, South Africa.

SN Applied Sciences (2019) 1:787 | https://doi.org/10.1007/s42452-019-0821-9

Received: 11 March 2019 / Accepted: 21 June 2019 / Published online: 26 June 2019

1 Introduction

The first synthetic dye, Mauve or Aniline-Purple, was discovered in 1856 [1]. Since this discovery, dyes have become an indispensable part of the textile- and many other industries [2]. Based on a review published in 2011 [2], there are more than 100,000 dyes available and more than a million tons of these dyes are produced each year. On average, 10–15% of these dyes end up in wastewater, which amounts to more than 300 mg/L of dye content [3]. This is cause for concern, since a dye content of only 1 mg/L is enough to visibly color effluents. Aside from the aesthetics of highly colored effluents, the harmful properties of the dyes are also problematic. In 2001, Nigam and co-workers published a review on the remediation of dyes in effluents from the textile industry [4], where they highlighted the same issues—the fact that the dyes are not only visible at very low concentrations, but they are harmful due to properties including toxicity, carcinogenicity and mutagenicity [5]. Furthermore, they emphasized that these dyes are generally resistant to the aerobic treatment process applied to municipal sewage water. This resistance to degradation along with the pollutant and other harmful properties poses a significant problem.

Currently, there are several approaches to treat highly colored effluent streams containing organic dye molecules. These methods fall into various categories including, chemical, physical and biological [2, 3, 6]. Although there has been a degree of success with these methods, there are problems with the implementation, including incomplete color removal or degradation and a lack of feasibility. Hence, current research is focused on developing more effective and less expensive methods for treating wastewater [4]. Since reductive degradation and/or discoloration has shown promise as a means of decoloring these effluents and generating less harmful materials, catalytic reductive discoloration was considered as a cheaper and possibly more efficient means of treating dye-containing effluents.

Literature studies have shown that supported gold nanoparticles are very efficient catalysts for the reduction of 4-nitrophenol [7, 8]. Chang and Chen reported one such example, where gold nanoparticles (3.14 nm) were loaded onto a magnetic nanocarrier with a chitosan coating. The chitosan provided the driving force for the formation and stabilization of the gold nanoparticles. The catalytic studied showed that the magnetically recoverable nanocatalyst could reduce 4-nitrophenol to 4-aminophenol in the presence of sodium borohydride within minutes and could be recycled up to eleven times without a significant loss in activity [7]. Similarly, unsupported gold nanoparticles have been used to catalyze reductive dye degradation [9–12]. Gold nanoparticles produced by various green synthetic methods and with sizes in the range of 10–50 nm have been employed to successfully reduce methylene blue, methyl orange and Congo red in the presence of sodium borohydride. Unlike their supported counterparts, the recyclability of these gold nanoparticles was not considered [9–12].

Since highly reactive small gold nanoparticles tend to agglomerate [9], stabilizers are required to ensure that agglomeration (and consequent deactivation) is prevented or limited. As demonstrated by the examples above, the supported gold nanoparticles are significantly smaller than their unsupported counterparts and the supported nanocatalysts generally display good recyclability due to their enhanced stability. Various support materials have been employed successfully to limit agglomeration for various applications. Among others, silica has proven to be an attractive support material because it is inexpensive and abundant with high stability [13, 14]. Furthermore, since silica has been employed as a sorbent material for treating wastewater [2] it is the ideal choice of support for active gold nanoparticles employed as dye degradation catalysts.

In this paper, the design, synthesis and evaluation of gold-decorated amino-functionalized silica nanoparticles (SS_x–AMPS–Au) as nanocatalysts for the reductive discoloration of methylene blue is discussed. To determine the full potential of these catalysts, the scope for reducing a range of anionic and cationic dyes was also evaluated.

2 Materials and methods

2.1 General

The chemicals used include tetraethyl orthosilicate (TEOS, 98%, Sigma-Aldrich), ammonium hydroxide (28–30%, Sigma-Aldrich), absolute ethanol (99.8%, Merck), ethanol (96.4%, Scienceworld), (3-aminopropyl) trimethoxysilane (AMPS, 97% Sigma-Aldrich), isopropanol (99.5%, Scienceworld), gold(III) chloride trihydrate ($HAuCl_4{\cdot}3H_2O$, ≥ 49.0%, Sigma-Aldrich), sodium borohydride ($NaBH_4$, 99.99%, Sigma-Aldrich), sodium citrate tribasic dihydrate (≥ 99.0%, Sigma-Aldrich) and fresh Type II water. The organic dyes employed were methylene blue (MB, > 96%, May & Baker Ltd.), methyl orange (MO, > 90%, Merck), rhodamine B (RB, > 90%, E. Gurr, Michrome), congo red (CR, > 90%, BDH Chemicals Ltd.), malachite green (MG, > 90%, Fluka) and crystal violet (CV, > 90%, BDH Chemicals Ltd.).

2.2 Preparation of silica nanoparticle cores and AMPS-functionalized silica nanoparticles, SS_x NPs and SS_x–AMPS NPs

The synthesis of the SS_x NPs was adapted from the method reported by Galembeck and co-workers [15] and the SS_x–AMPS NPs were synthesized by modifying the method reported by Mulvaney and co-workers [16]. General methods are described in the supporting information.

2.3 Preparation of SS_x–AMPS–Au_n nanoparticles with various gold loadings (n) and silica core sizes (x)

2.3.1 SS_{20}–AMPS–Au_n NPs for n = 5, 10 and 15

The most suitable gold loading for the SS_x–AMPS NPs was determined by using the method reported below and varying the gold loading (5–15 mM). Details are provided in the supporting information.

2.3.2 SS_x–AMPS–Au_{10} NPs for x = 20, 50 and 100

SS_x–AMPS NPs (50 mg) were isolated from the stock solution by centrifugation (15,000 rpm × 30 min). The supernatant was decanted and replaced with water (8 mL). Next, the particles were resuspended by sonication to form a silica suspension. Water (17 mL) and the silica suspension (8 mL) were added to a round bottom flask. The flask was stoppered, and the solution was stirred magnetically for 5 min at 300 rpm and 25 °C. Next, a 10 mM gold solution was prepared (17 mg $HAuCl_4$ in 5 mL H_2O). 10 mM gold stock solution (2.5 mL) was added to the flask. The flask was stoppered again, and the reaction was stirred for 2 h. Thereafter, a 100 mM $NaBH_4$ solution was prepared (19 mg $NaBH_4$ in 5 mL H_2O). The $NaBH_4$ solution (2 mL) was added dropwise via a syringe pump at a rate of 24 mL/h. Once the addition was complete, the solution was stirred for 30 min. SS_x–AMPS–Au NPs were isolated by centrifugation at 15,000 rpm for 30 min. The supernatant was decanted, and the pellets were washed by adding water (8 × 1.5 mL/tube) and sonicating the tubes (1–3 min) to resuspend the silica. After washing, the silica was isolated by centrifuging again (15,000 rpm for 30 min). The supernatant was decanted, and the SS_x–AMPS–Au NPs were resuspended in water (1.0 mL/tube) and diluted with water to obtain a stock solution (30 mL).

2.4 Dye discoloration

The method reported by Saikia et al. [17] was used as a starting point. General methods are provided here for the reductive discoloration of methylene blue.

The following stock solutions were prepared with Type II water and stored at room temperature (25 °C): 1 mM methylene blue and 50 mM $NaBH_4$. The stock solutions of the SS_x–AMPS–Au catalysts were prepared by diluting the original solutions so that 1–2 mol% gold relative to the dyes could be achieved. Note that if the original solution was not in water, the required mass of particles was isolated by centrifugation and then resuspended in water. Next, samples for UV–Vis spectroscopic analysis of the catalysis reaction were prepared using the stock solutions. Concentrations provided in brackets are the final concentration in the samples.

2.5 General sample preparation method for reductive discoloration of methylene blue

The following were added to a cuvette to achieve a total volume of 3000 µL: methylene blue (120 µL; 0.040 mM), water (1867–2551 µL), nanoparticles (326–353 µL, 1–2 mol% gold relative to substrate as indicated, or an equivalent silica loading (µg/µL) for the naked and functionalized silica samples). The cuvette was then placed in the UV–Vis spectrophotometer with the cell holder temperature set to 25 °C (unless specified otherwise). The $NaBH_4$ (2.4–660 µL; 0.040 mM–11 mM; 1–275 equivalents relative to substrate) was added and the mixture was stirred quickly. The UV–Vis spectroscopy absorbance was recorded in the range of 800–200 nm or at the λ_{max} for the dye at 15 s intervals. Note that the λ_{max} for each dye was determined beforehand. For all UV–Vis spectroscopy data sets, the raw data were exported to Excel and processed further. All experiments were performed in triplicate and the results were averaged, unless otherwise specified.

3 Results and discussion

3.1 Design, synthesis and characterization

Taking inspiration from the literature [14, 18–20], gold-decorated amino-functionalized silica nanoparticles (SS_x–AMPS–Au) were designed as potential dye discoloration catalysts. The rationale behind the design is that the amino-functionalized silica cores will stabilize the active gold nanoparticles thus, limiting agglomeration and possibly improving the activity. A three-step synthesis was developed with a focus on repeatability and ease (Fig. 1). Initially, Stöber methods [21] were used to generate a range of silica cored nanoparticles (20–100 nm) via an optimized method, where only one reagent is varied. Next, the silica nanoparticle cores were functionalized with (3-aminopropyl)trimethoxysilane (AMPS) [16]. Finally, the decoration of the nanoparticle cores with gold

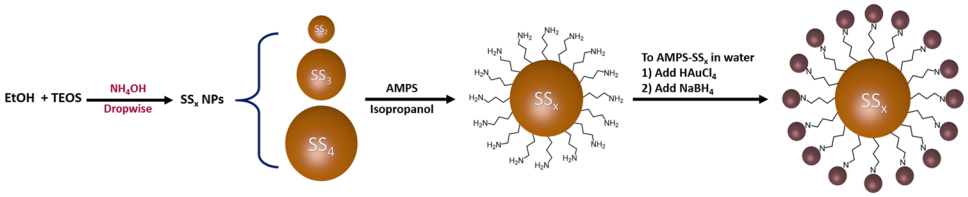

Fig. 1 Synthetic scheme for SS_x–AMPS–Au nanoparticles

nanoparticles (2–5 nm) was achieved via a simple deposition–precipitation process [22].

For the silica cores, three sizes were prepared (20, 50 and 100 nm) so that the effect of the core size could be determined. Modifying the method reported by Galembeck and co-workers [15], the desired core sizes could be achieved by varying the amount of ammonium hydroxide added. Characterization by TEM microscopy confirmed the formation of roughly spherical particles with the sizes 16 nm, 50 nm and 102 nm, respectively. As expected, the size decreased with decreasing ammonium hydroxide concentration. Furthermore, it was noted that the shape becomes more irregular as the particle size decreases. Similarly, the dispersion of the particles decreased with the size. Therefore, the smaller particles aggregated into large clusters due to the high surface area and consequently high reactivity.

The next step was to functionalize the silica with AMPS. Following the method reported by Mulvaney et al. [16], AMPS-functionalized silica (SS_x–AMPS) nanoparticles were obtained. The AMPS loading was varied to (theoretically) achieve the same AMPS/surface area coverage on all particles. UV–Vis spectra were recorded and clearly showed the $–NH_2$ band at approximately 280 nm.

The final step of the synthesis involved loading gold onto the functionalized-silica cores. This was done by a deposition–precipitation method adapted from the literature [22]. Preliminary tests showed that a 10 wt % gold loading is the most efficient with respect to the particle size and size-distribution of the gold nanoparticles (Figure S3—Supporting information). Again, UV–Vis spectroscopy was employed to determine if the synthesis was successful. The spectra for each stage of the synthesis are shown in Fig. 2.

For the gold-decorated silica nanoparticles (SS_x–AMPS–Au), the $–NH_2$ absorbance is observed at approximately 260 nm. This is a shift of approximately 20 nm from the SS_x–AMPS $–NH_2$ band due to the interaction of the $–NH_2$ groups with gold. The surface plasmon resonance (SPR) absorbance appears as a broad absorbance in the range of 520 nm, confirming the formation of gold nanoparticles. With increasing silica size, the SPR peak undergoes a slight red shift. This suggests that the gold nanoparticle size increases with the silica size, albeit very slightly [23]. Furthermore, the absence of the gold ion

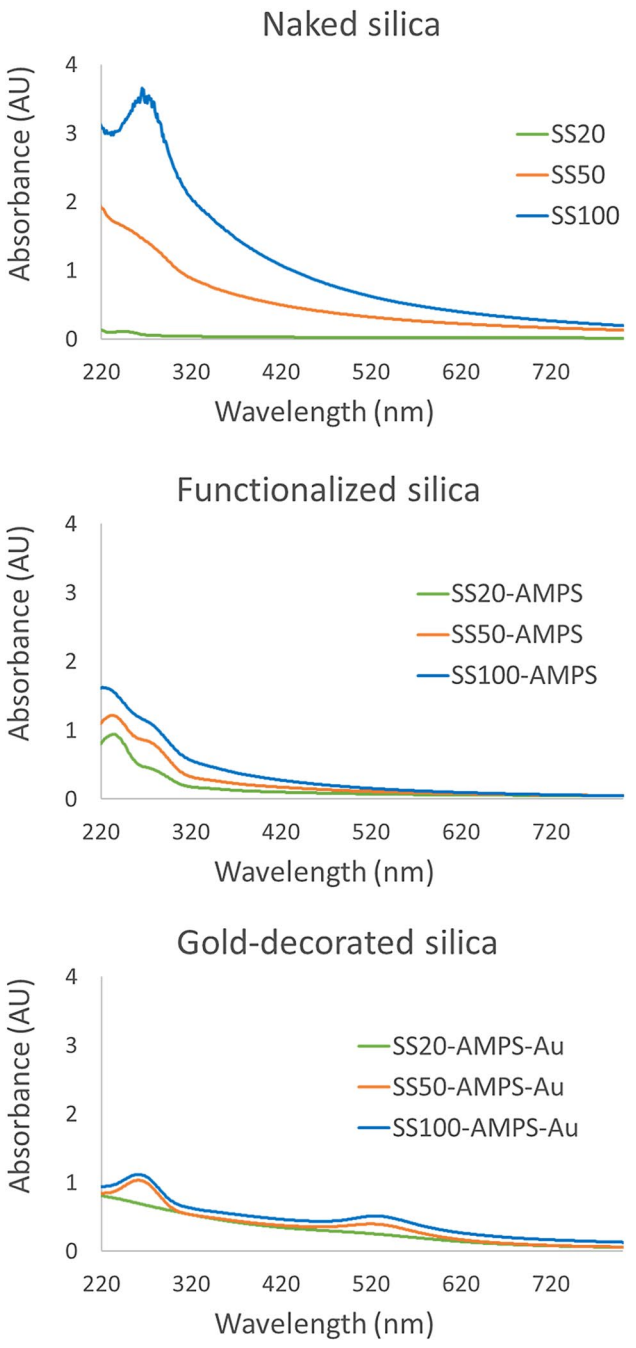

Fig. 2 UV–Vis spectra for the nanoparticles after each of the 3 steps for the synthesis of SS_x–AMPS–Au nanoparticles

absorbance at 300 nm confirms complete reduction of the $HAuCl_4$ salt to gold nanoparticles.

Next, TEM microscopy was used to determine the size and morphology of the particles. The micrographs show roughly spherical silica cores decorated with gold nanoparticles. Since the gold nanoparticles do not form a complete layer, the structure is referred to as a raspberry-like particle rather than a core–shell structure [16]. Hence, the structure is denoted as SS_x–AMPS–Au, where SS_x represents the silica cores with varying size (x), AMPS is the (3-aminopropyl)trimethoxysilane linker and Au represents gold nanoparticles on the surface. Representative micrographs are shown in Fig. 3, along with histograms showing the particle size distribution and average particle size for both the silica and the gold nanoparticles. As predicted, the smallest silica (with the largest surface area) provided the highest degree of stabilization for the gold nanoparticles, thus the gold nanoparticles on the small silica cores are the smallest and those on the largest silica cores are the largest (due to the relatively lower degree of stabilization). This supports the UV–Vis spectroscopy findings. It is worth noting that the dispersion of the modified nanoparticles is not quite as good as the dispersion of the naked silica nanoparticles (Figure S5—Supporting information). The change may be due to the surface modification or an increase in concentration of particles in solutions, following the purification steps. Hence, the stability of the particles will be determined, as discussed later on.

In addition to the micrographs, TEM-EDS was performed to confirm the presence of all elements (Figure S4—Supporting information). All nanoparticles showed Si and O from the SiO_2 silica core and Au from the gold nanoparticles on the surface. The C and N from the AMPS linker could not be detected due to the low concentration relative to the other elements. However, the presence of metallic gold supports the SS_x–AMPS–Au raspberry-type

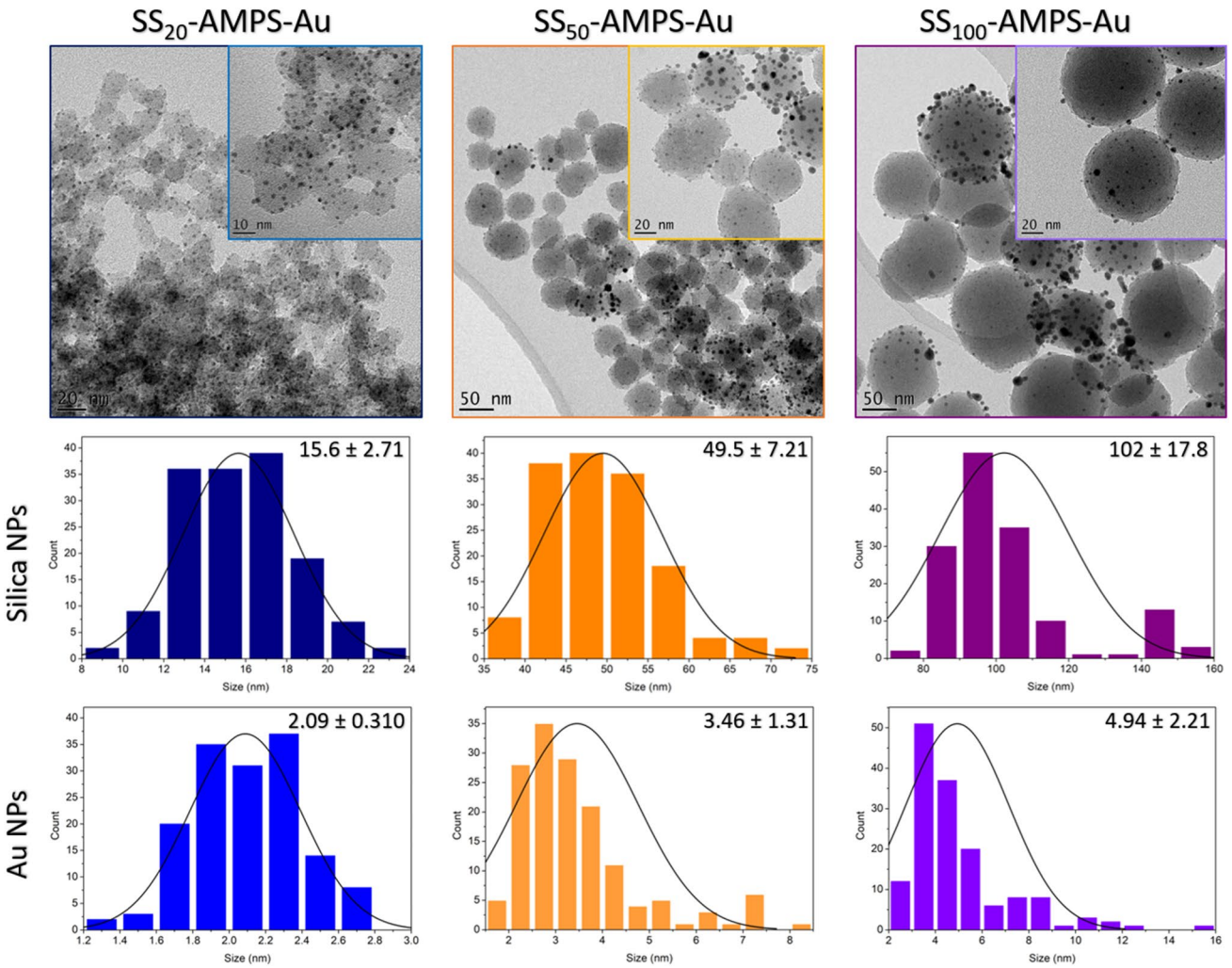

Fig. 3 TEM micrographs and histograms showing particle size distribution for SS_x–AMPS–Au nanoparticles

structures observed in the TEM micrographs. Following TEM microscopy, the metal content was determined with ICP-AES (Table S2—Supporting information). The loadings achieved varied with the silica size, however, the actual percentage of gold loaded (compared to the theoretical loading) was approximately 80%.

Once the synthesis and characterization were complete, the next step was to evaluate the success of the design. Hence, the stability and catalytic activity of these raspberry-like SS_x–AMPS–Au nanoparticles were investigated by employing the nanoparticles as reductive dye degradation catalysts.

3.2 Stability over time

Once synthesized, the particles were stored as aqueous suspensions in a dark cupboard at room temperature. After 3 months, the solutions were sonicated and fresh TEM samples were prepared and analyzed. The initial TEM micrographs and histograms are compared with those obtained after 3 months shown in Fig. 4.

From the repeat TEM micrographs, it was clear that the larger particles are stable, showing little to no change. As expected, the smaller particles are less stable and tend to slightly aggregate. Overall, the gold nanoparticles were quite stable whilst the silica nanoparticles showed more size variation. The small SS_{20} nanoparticles aggregated to the extent that the particle size could not be determined accurately, whilst the larger SS_{50} and SS_{100} nanoparticles showed slight aggregation. Based on the TEM micrographs, it is thought that the gold nanoparticles are adequately stabilized on the SS_x–AMPS nanoparticles, but the aggregation of these core particles brings the gold nanoparticles into contact with one another, thus, facilitating agglomeration. A schematic representation of this is shown in Fig. 5. Hence, the medium sized silica core structure, SS_{50}–AMPS–Au, provides the best balance between stability and small gold nanoparticle size for catalytic applications. A way in which to limit the aggregation of the core particles in future, may be to increase the amine loading on the surface, thus preventing the core particles for coming into contact or incorporating an amine with a longer aliphatic chain for the same purpose.

3.3 Reductive discoloration of methylene blue

The reductive discoloration of methylene blue was carried out as a model reaction for the discoloration of cationic dyes. Initial optimization studies were carried out using similar conditions to those reported by Saikia et al. [17].

For each catalyst, the catalyzed reaction, as well as several control reactions were carried out. The composition of these reactions is shown in Table 1.

Based on optimization reactions, the initial catalytic conditions for a methylene blue discoloration reaction at 25 °C were: 40 uM methylene blue, 2 mol% gold and 275

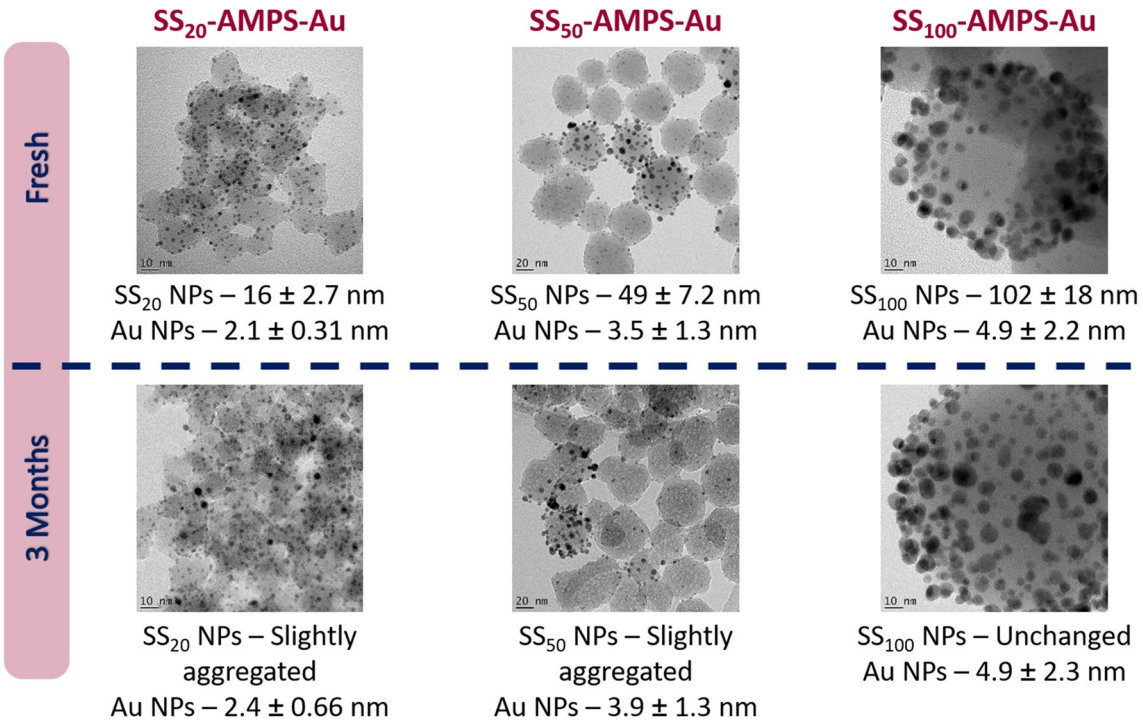

Fig. 4 TEM micrographs of SS_x–AMPS–Au nanoparticles after preparation (top) and after 3 months (bottom)

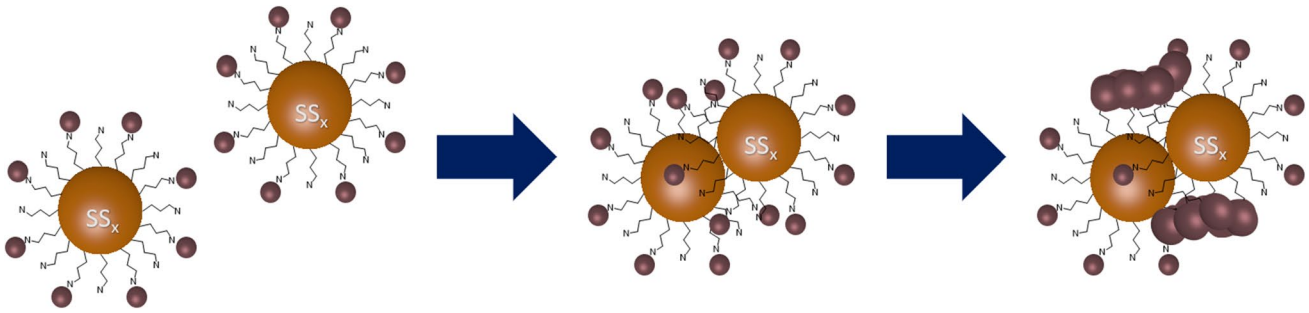

Fig. 5 Schematic representation of proposed agglomeration of Au nanoparticles on SS_x–AMPS cores

Table 1 Composition of catalyzed reaction and various control reactions for each catalytic test

Control reaction	Dye	Reducing agent	Catalyst (SS_x–AMPS–Au)	Functionalized silica (SS_x–AMPS)	Silica (SS_x)
B1	x				
B2	x		x		
B3	x	x			
SS	x	x			x
AMPS	x	x		X	
Au	x	x	x		

equivalents of reducing agent ($NaBH_4$). Figure 6a, b shows the absorbance for methylene blue ($\lambda_{max} = 663$ nm) for each of the reactions run for the SS_{100}–AMPS–Au catalyst, as well as the percentage reduction achieved.

From Fig. 6a, b, it was determined that no reduction occurred for control reactions B1 and B2. The absence of reduction for B1 shows that the dye is stable for the reaction period and does not reduce by itself. The unchanged absorbance for B2 shows that the catalyst cannot reduce the dye in the absence of reducing agent. A small percentage (< 10%) of reduction was observed for reactions B3, SS and AMPS (see inset in Fig. 6b). These reactions contained reducing agent, but no catalyst. Hence, the dye can be reduced by reducing agent, but over a significantly longer period and the reduction is incomplete (max. 50%). The only reaction that showed complete discoloration of methylene blue within 900 s was the reaction that was catalyzed in the presence of reducing agent. Complete reduction was achieved within 300 s, whilst the uncatalyzed reactions showed a maximum of 7% reduction in 900 s. Hence the addition of the catalysts significantly enhances the rate of the reduction reaction.

Next, the three different catalysts were compared, under the optimized conditions, to determine the effect of the silica nanoparticle size. Figure 7 shows the percentage reduction achieved by each of the three catalysts over a 15 min period. The graph in Fig. 7 clearly

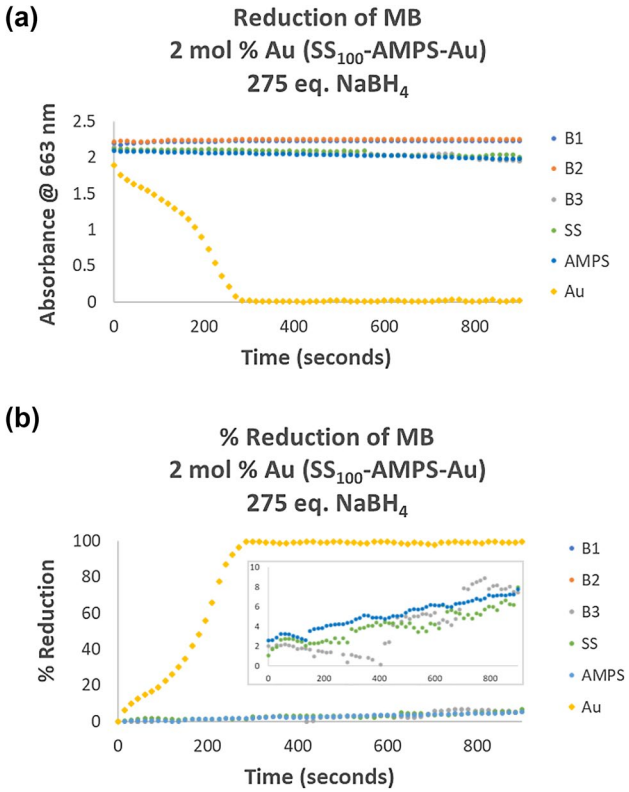

Fig. 6 **a** Absorbance values at 663 nm for methylene blue discoloration by SS_{100}–AMPS–Au catalyst and control reactions (top) and **b** corresponding percentage reduction (bottom)

demonstrates that there is a difference in the rate at which methylene blue is reduced by each catalyst. The rate of the reaction was slowest for catalyst on the larger silica support (SS_{100}) and fastest for the medium sized silica support (SS_{50}). What was interesting was that the smallest silica support with the smallest gold nanoparticles (SS_{20}) was not the best catalyst. Theoretically, the increased surface area of the small SS_{20} nanoparticles provides a large silica surface for stabilization of the Au nanoparticles. Thus, producing small, highly reactive Au nanoparticles as catalytic sites. This lower activity may

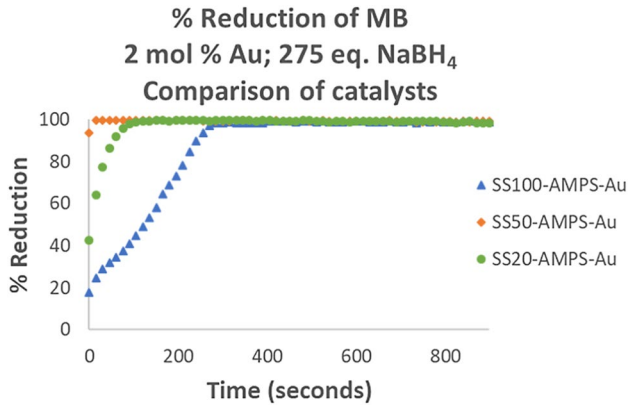

Fig. 7 Calculated % reduction of methylene blue for the three catalysts with 275 equivalents $NaBH_4$

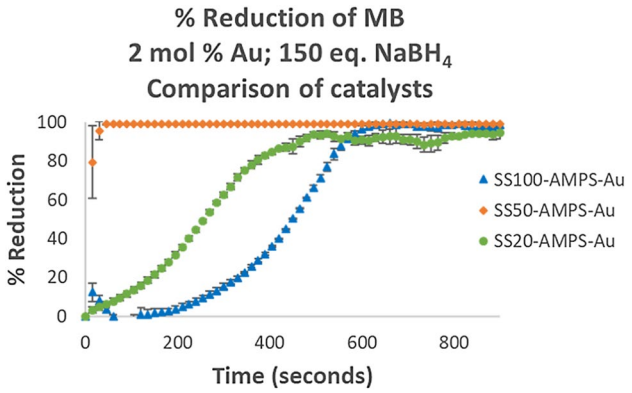

Fig. 8 Calculated % reduction of methylene blue for the three catalysts with 150 equivalents $NaBH_4$

Table 2 Selected characterization data for SS_x–AMPS–Au catalysts for comparison with catalytic trends

Property	SS_{20}–AMPS–Au	SS_{50}–AMPS–Au	SS_{100}–AMPS–Au
Catalytic rate	Medium	Fast	Slow
Silica size (nm)	15.6 ± 2.71	49.5 ± 7.21	102 ± 17.8
Au size (nm)	2.09 ± 0.305	3.46 ± 1.31	4.94 ± 2.21
Au loading (mg/mL)	0.145	0.108	0.134
Au loading (%)	79.9	66.1	81.5

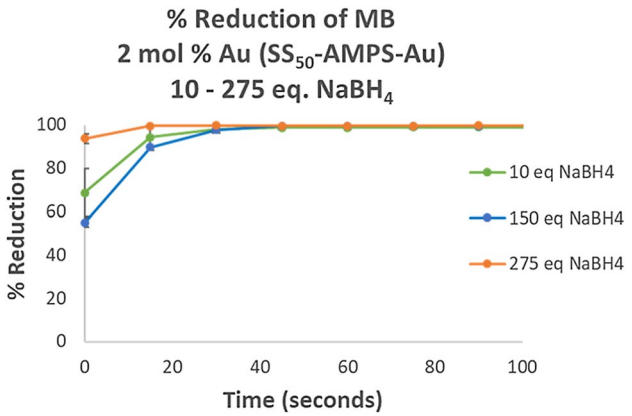

Fig. 9 Calculated % reduction of methylene blue for the three catalysts with varying equivalents of $NaBH_4$

be due to agglomeration, as observed in the TEM micrographs (Fig. 4).

Based on the characterization data in Table 2, the catalytic trend (Table 2, row 1) matches the gold loading percentage (Table 2, row 5). Therefore, the catalyst with the lowest gold loading (percentage) has the lowest surface coverage. Hence, it is proposed that there is more exposed gold surface for the reaction to occur, especially since the dye molecules are quite large. These results correlated with the proposed best catalyst in Sect. 3.2, where the stability of the catalysts was considered.

The next step was to further optimize the reaction. Hence, in an attempt to make the reaction as green as possible, the equivalents of reducing agent were decreased. Figure 8 shows the results from the optimized reactions where only 150 equivalents of $NaBH_4$ were added.

From Fig. 8, the SS_{100}–AMPS–Au catalyst achieved 100% reduction after 300 s. Next, the SS_{20}–AMPS–Au catalyst achieved complete reduction after approximately 150 s. Again, the best results were obtained with the SS_{50}–AMPS–Au catalyst that reached 100% reduction in less than 20 s.

As the two weaker catalysts (SS_{100}–AMPS–Au and SS_{20}–AMPS–Au) were showing fluctuations in the absorbance due to insufficient mixing, further optimization was only carried out with the SS_{50}–AMPS–Au catalyst. A further decrease in the reducing agent was attempted. Figure 9 shows that a significant reduction in the $NaBH_4$ (275 equivalents to 10 equivalents) only slows the rate of the reaction slightly. This reduction in the reducing agent excess greatly improves the atom economy by reducing waste products. The consequent cost reduction is also beneficial.

Since the rate of the reaction was still very fast, further rate reduction using $NaBH_4$ and the catalyst loading were tested, however, these attempts were not successful, as the absorbance values fluctuated throughout the reaction time. To probe this, a spectrum scan was performed to obtain more information, as shown in Fig. 10a.

The spectra showed that methylene blue (λ_{max} = 663 nm) is reduced to leuco methylene blue (λ_{max} = 256 nm), but an equilibrium is established (Fig. 10b). Hence, the addition of more reducing agent and or a higher catalyst loading is required to achieved complete reduction. Increasing

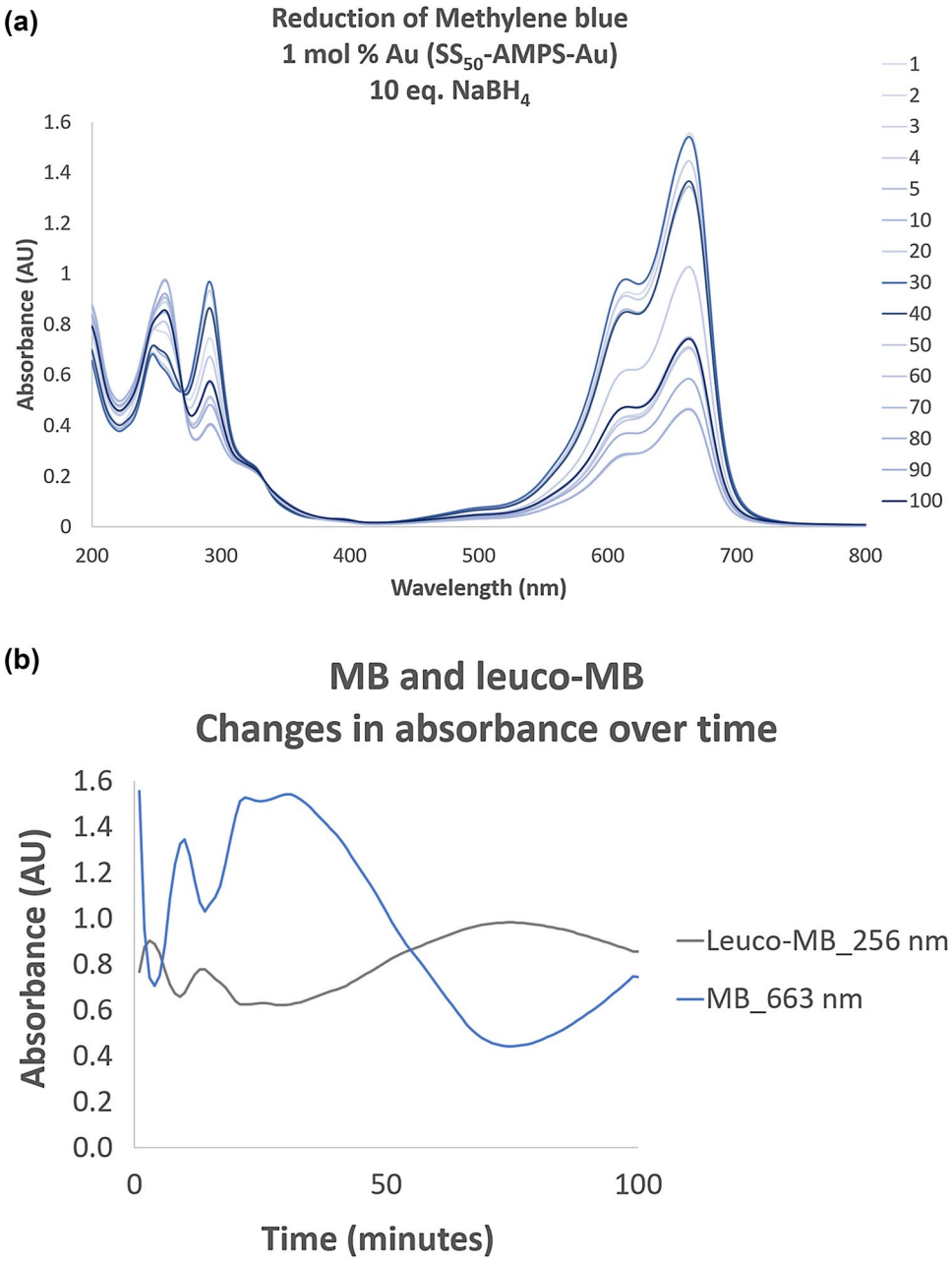

Fig. 10 **a** Spectrum showing a possible equilibrium state between methylene blue reduction and oxidation and **b** changes in absorbance at 663 nm (methylene blue) and 256 nm (leuco-methylene blue)

the catalyst loading by 1% is likely greener than adding a significant excess of the reducing agent, therefore, the chosen optimized conditions are 40 µM methylene blue, 2 mol% gold and 10 equivalents of reducing agent. Under these conditions, the SS_{50}–AMPS–Au catalyst achieved 100% reduction of methylene blue to leuco methylene blue within 50 s (Fig. 9). A comparison of the three catalysts at the optimized conditions showed incomplete reduction by SS_{20}–AMPS–Au and SS_{100}–AMPS–Au with only SS_{50}–AMPS–Au achieving complete conversion. SS_{20}–AMPS–Au and SS_{100}–AMPS–Au showed initial reduction, followed by an increase in the absorbance, suggesting that the reduction reaction was reversed. This again speaks to the formation of an equilibrium. This is likely due to a weak interaction between the substrate and the catalyst.

3.4 Recycling of catalyst

For green catalysts and nanocatalysts, recyclability is an important and valuable property. Based on the incorporation of the silica cores to enhance the stability of the gold nanoparticles, these catalysts should be easily recyclable.

In order to evaluate recyclability, the discoloration of methylene blue was catalyzed under optimized conditions. Once complete, the catalyst was isolated from the

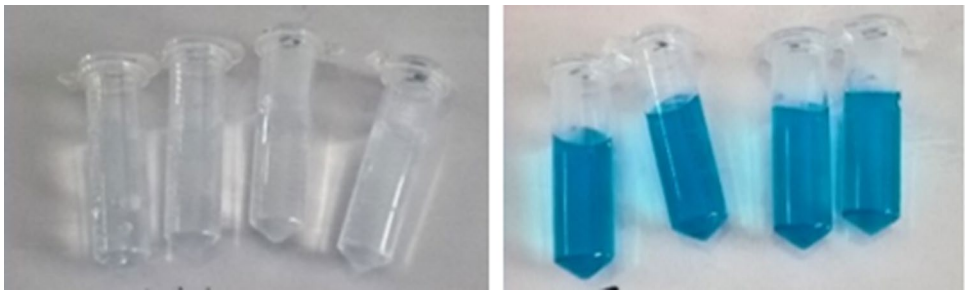

Fig. 11 Reaction mixture after reduction (left) and after catalyst isolation (right)

solution by centrifugation. However, oxidation of the leuco-methylene blue to methylene blue occurs upon isolation of the catalyst, as shown in Fig. 11. During the optimization studies, it was noted that the use of too little catalyst or reducing agent resulted in an equilibrium, where the oxidation and reduction reactions occur reversibly. Hence, the removal of the catalyst from the system may promote a reversal of the reduction reaction. Thus alternative conditions in which to drive the reduction reaction forward, were considered.

Therefore, the recyclability test was repeated with more reducing agent (275–625 equivalents of $NaBH_4$) and higher gold loadings (2–10 mol%). Despite the large excess of reducing agent and/or increased gold loading, the dye was re-oxidized upon isolation of the catalyst. Increased reaction temperature (25–45 °C) also proved ineffective.

As a final test, non-catalytic conditions were employed. There are literature reports where non-catalytic quantities of metal (> 10 mol% metal) have been employed successfully [9, 12, 17], hence, the catalyst loading was increased to 50 mol% Au and the reducing agent was kept at 275 equivalents. These conditions are similar to those employed by Das and co-workers [17]. This reaction is a metal-mediated system, rather than a metal-catalyzed system. The initial reaction, with fresh catalyst, showed complete conversion from methylene blue to leuco-methylene blue. The catalyst was then isolated from the reaction solution by centrifugation. The supernatant was decanted and monitored over time (Fig. 12) and found to convert back to methylene blue when left overnight in the absence of catalyst. The isolated catalyst pellet was resuspended in water. Fresh dye and reducing agent were added and the catalysis reaction was carried out. Again, complete reduction of methylene blue was observed (Fig. 13). However, isolation of the catalysts for a second time led to oxidation of the desired leuco-methylene blue, back to methylene blue. Hence, the nanoparticles can be recycled once in this system.

Both catalytic- and metal-mediated reactions showed complete reduction of methylene blue, but only the nanoparticles from the metal-mediated reaction could be recycled. Table 3 shows a comparison of

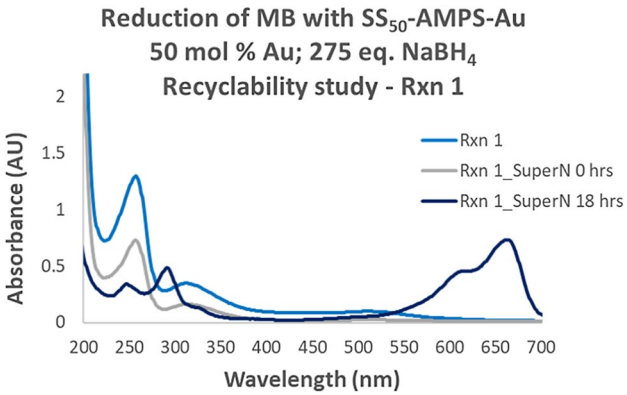

Fig. 12 UV–Vis spectra of the initial catalysed reaction (Rxn 1) showing only leuco-MB and the supernatant (Rxn 1_SuperN) over time which oxidizes from leuco-MB to MB

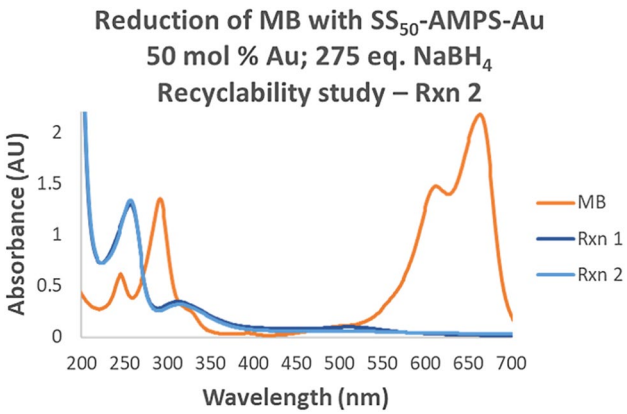

Fig. 13 UV–Vis spectra showing MB (MB) and the initial reduction of MB with fresh catalyst (Rxn 1), as well as the reduction of MB by recycled catalyst (Rxn 2)

the catalytic- and metal-mediated reaction conditions. It is quite clear that although the catalytic system is not recyclable, it is a far greener method than the metal-mediated reductive discoloration. Not only does the catalytic system have a better atom economy, but it is also significantly less expensive.

Table 3 Comparison of catalytic and metal-mediated reaction conditions

Reagent	Catalytic reaction	Metal-mediated reaction
Mol% Au SS_3–AMPS–Au	2	50
$NaBH_4$ (no. of equivalents)	10	275
Recyclability (total no. of cycles)	1	2

3.5 Mechanism for reductive dye discoloration

From the literature, it is proposed that metal nanoparticles act as electron transfer systems, facilitating the transfer of an electron from $NaBH_4$ to the dye. The transfer process in unfavourable due to a large potential difference between the reagents. Hence, metal nanoparticles, with an intermediate potential assists in the transfer of the electron [9]. In order to confirm the mechanism, the same reaction conditions as above were applied, however, fresh reducing agent was not added upon recycling of the catalyst. Complete reduction of the dye was achieved, as in the initial reaction with fresh catalyst. This observation suggests that the electrons are transferred from $NaBH_4$ to the catalyst surface in the initial reaction and the excess electrons remaining on the catalyst surface then reduce the dye in the second reaction, thus confirming that SS_{50}–AMPS–Au follows the proposed mechanism, as shown in Fig. 14.

3.6 Reductive dye discoloration of other dyes

Since many different dyes end up in waste streams, these catalysts were evaluated for their ability to reduce a range of both cationic and anionic dyes. Figure 15 summarizes the percentage reduction achieved with each of the three catalysts, as well as the reduction achieved with only reducing agent (in the absence of catalyst). The aim of this

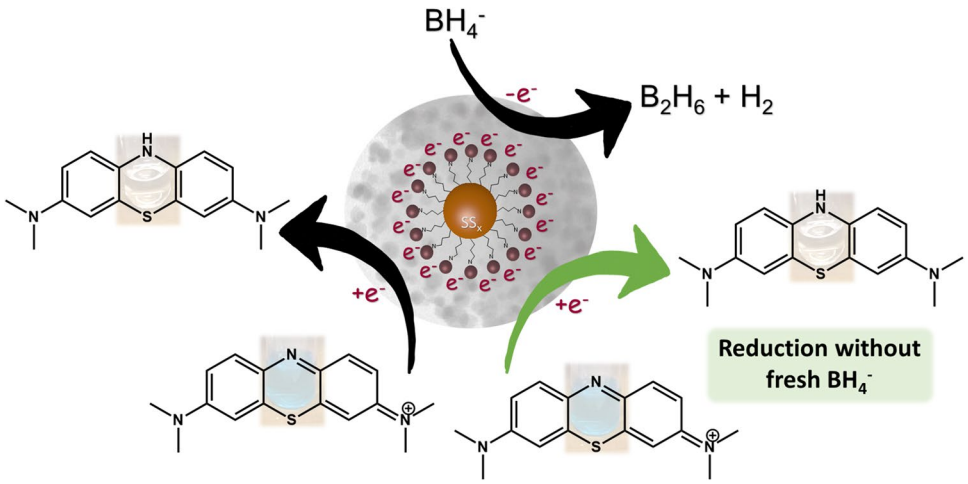

Fig. 14 Proposed electron transfer mechanism reported in the literature, where electrons from $NaBH_4$ are transferred to methylene blue via the catalyst surface. By recycling the catalyst in the absence of $NaBH_4$, methylene was reduced by electrons already on the catalyst surface from the previous reaction

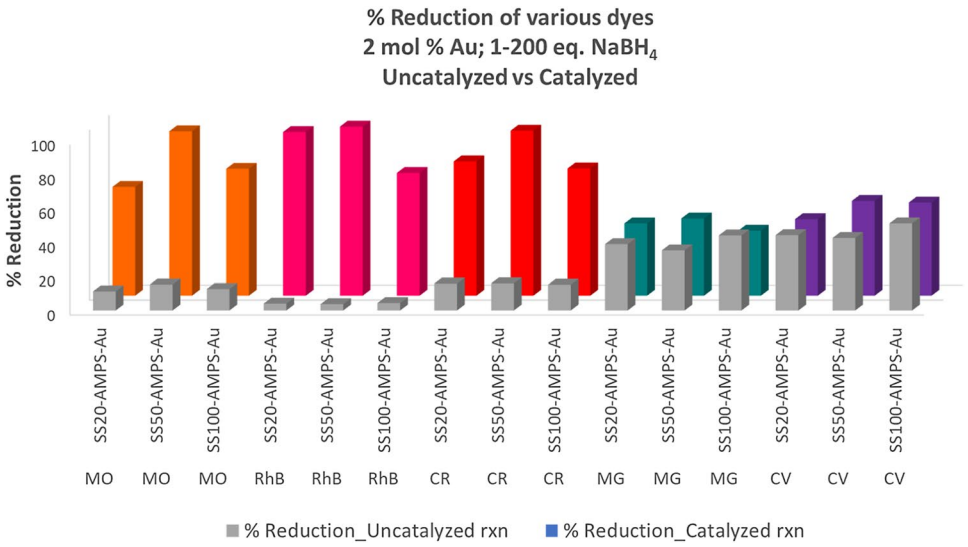

Fig. 15 Reduction of cationic and anionic dyes by SS_x–AMPS–Au catalysts with 2 mol% Au and 1, 5 or 200 equivalents $NaBH_4$ for MG, CV and remaining dyes, respectively

assay was to demonstrate the scope of these catalysts for the reductive discoloration of a range of organic dyes.

The anionic dyes, methyl orange (MO) and congo red (CR) were successfully reduced. Similarly, the cationic dyes, rhodamine B (RhB), malachite green (MG) and crystal violet (CV) were also reduced. Malachite green and crystal violet were easily reduced with 1–5 equivalents of $NaBH_4$ (in the absence of catalyst), and the addition of catalysts did not appear to have a significant advantage.

Irrespective of the dye, SS_{50}–AMPS–Au was the most efficient catalyst. Interestingly, MO, RhB and CR were more difficult to reduce than MB, but almost complete reduction was achieved in 15 min using 2 mol% Au and 200 equivalents of $NaBH_4$. Based on results in Fig. 15, the SS_x–AMPS–Au nanocatalysts are efficient dye discoloration catalysts for both cationic and anionic dyes.

4 Conclusion

In this paper, SS_x–AMPS–Au nano-raspberries were synthesized by a 3-step method with facile and reproducible techniques. The naked silica spheres (SS_x) ranged of approximately 20–100 nm in size, whilst the discrete gold nanoparticles (Au) on the functionalized silica (SS_x–AMPS) were in the range of 2–5 nm.

Application of these nano-raspberries in dye discoloration studies, showed that the SS_x–AMPS–Au nano-raspberry design has promise for application as electron transfer systems for reductive discoloration of a range of organic dyes. Not only are the nanoparticles stable for at least 3 months, but they are also easily isolated from the reaction system. Both catalytic- and metal-mediated reactions showed complete reduction of methylene blue. Comparison of the catalytic- and metal-mediated reaction conditions showed that the catalytic system was the greener of the two systems with respect to atom economy and cost, despite it not being recyclable. The most efficient catalyst was the SS_{50}–AMPS–Au nanocatalyst, with a 50 nm silica core and gold nanoparticles of 3.5 nm. Under optimized conditions, SS_{50}–AMPS–Au induced complete reduction of methylene blue in less than 20 s at room temperature, using only 10 equivalents of reducing agent. At the same catalyst loading, SS_{20}–AMPS–Au and SS_{100}–AMPS–Au catalysts required at least 150 equivalents of reducing agent to achieve complete reduction within 900 s. It is likely the balance between the nanoparticle stability, dispersion and the smaller size of the gold nanoparticles that makes the SS_{50}–AMPS–Au nanoparticle system such a good catalyst compare to its counterparts. Hence, this class of SS_x–AMPS–Au nanocatalysts presents a promising starting point for the development of green catalytic (and metal-mediated) systems for reductive dye discoloration, where the silica core particle size and amine loading can be tailored to achieve good dispersion and small, stable gold nanoparticles to yield optimum catalytic efficiency.

Acknowledgements The financial assistance of the National Research Foundation (NRF) (Grant No. GEP180116305797) towards this research is hereby acknowledged. Opinions expressed, and conclusions arrived at, are those of the author and are not necessarily to be attributed to the NRF.

Compliance with ethical standards

Conflict of interest On behalf of all authors, the corresponding author states that there is no conflict of interest.

References

1. Perkin WH (1863) On mauve or aniline-purple. Proc R Soc Lond 12:713–715
2. Singh K, Arora S (2011) Removal of synthetic textile dyes from wastewaters: a critical review on present treatment technologies. Crit Rev Environ Sci Technol 41:807–878. https://doi.org/10.1080/10643380903218376
3. Marcucci M, Ciabatti I, Matteucci A, Vernaglione G (2003) Membrane technologies applied to textile wastewater treatment. Ann N Y Acad Sci 984:53–64. https://doi.org/10.1111/j.1749-6632.2003.tb05992.x
4. Robinson T, Mcmullan G, Marchant R, Nigam P (2001) Remediation of dyes in textile effluent: a critical review on current treatment technologies with a proposed alternative. Bioresour Technol 77:247–255
5. Houk VS (1992) The genotoxicity of industrial wastes and effluents. A review. Mutat Res Genet Toxicol 277:91–138. https://doi.org/10.1016/0165-1110(92)90001-p
6. Patel H, Vashi RT (2015) Characterization of textile wastewater. In: Characterization and treatment of textile wastewater. Elsevier Inc., Waltham, pp 21–71. https://doi.org/10.1016/B978-0-12-802326-6.09996-2
7. Chang YC, Chen DH (2009) Catalytic reduction of 4-nitrophenol by magnetically recoverable Au nanocatalyst. J Hazard Mater 165:664–669. https://doi.org/10.1016/j.jhazmat.2008.10.034
8. Saha S, Pal A, Kundu S, Basu S, Pal T (2010) Photochemical green synthesis of calcium-alginate-stabilized Ag and Au nanoparticles and their catalytic application to 4-nitrophenol reduction. Langmuir 26:2885–2893. https://doi.org/10.1021/la902950x
9. Gupta N, Singh HP, Sharma RK (2011) Metal nanoparticles with high catalytic activity in degradation of methyl orange: an electron relay effect. J Mol Catal A Chem 335:248–252. https://doi.org/10.1016/j.molcata.2010.12.001
10. Suvith VS, Philip D (2014) Catalytic degradation of methylene blue using biosynthesized gold and silver nanoparticles. Spectrochim Acta Part A Mol Biomol Spectrosc 118:526–532. https://doi.org/10.1016/j.saa.2013.09.016
11. Ganapuram BR, Alle M, Dadigala R, Dasari A, Maragoni V, Guttena V (2015) Catalytic reduction of methylene blue and Congo red dyes using green synthesized gold nanoparticles capped by *Salmalia malabarica* gum. Int Nano Lett 5:215–222. https://doi.org/10.1007/s40089-015-0158-3
12. Umamaheswari C, Lakshmanan A, Nagarajan NS (2018) Green synthesis, characterization and catalytic degradation studies of gold nanoparticles against congo red and methyl

orange. J Photochem Photobiol B Biol 178:33–39. https://doi.org/10.1016/j.jphotobiol.2017.10.017
13. Polshettiwar V, Varma RS (2010) Green chemistry by nano-catalysis. Green Chem 12:743–754. https://doi.org/10.1039/b921171c
14. Jadhav SA (2014) Incredible pace of research on mesoporous silica nanoparticles. Inorg Chem Front 1:735–739. https://doi.org/10.1039/C4QI00118D
15. Costa CAR, Leite CAP, Galembeck F (2003) Size dependence of Stöber silica nanoparticle microchemistry. J Phys Chem B 107:4747–4755. https://doi.org/10.1021/jp027525t
16. Pastoriza-santos I, Gomez D, Perez-Juste J, Liz-Marzan LM, Mulvaney P (2004) A Simple effective medium approach. Phys Chem Chem Phys 6:5056–5060
17. Saikia P, Miah AT, Das PP (2017) Highly efficient catalytic reductive degradation of various organic dyes by Au/CeO_2-TiO_2 nanohybrid. J Chem Sci 129:81–93. https://doi.org/10.1007/s12039-016-1203-0
18. Stratakis M, Garcia H (2012) Catalysis by supported gold nanoparticles: beyond aerobic oxidative processes. Chem Rev 112:4469–4506. https://doi.org/10.1021/cr3000785
19. Liu B, Zhang W, Feng H, Yang X (2011) Rattle-type microspheres as a support of tiny gold nanoparticles for highly efficient catalysis. Chem Commun 47:11727. https://doi.org/10.1039/c1cc13717d
20. Liz-Marzan LM, Giersig M, Mulvaney P (1996) Synthesis of nanosized gold–silica core–shell particles. Langmuir 7463:4329–4335. https://doi.org/10.1021/la9601871
21. Stober W, Fink A (1968) Controlled growth of monodisperse silica spheres in the micron size range 1. J Colloid Interface Sci 26:62–69
22. Du X, He J (2012) Amino-functionalized silica nanoparticles with center-radially hierarchical mesopores as ideal catalyst carriers. Nanoscale 4:852–859. https://doi.org/10.1039/c1nr11504a
23. Mühlig S, Rockstuhl C, Yannopapas V, Bürgi T, Shalkevich N, Lederer F (2011) Optical properties of a fabricated self-assembled bottom-up bulk metamaterial. Opt Express 19:9607–9616. https://doi.org/10.1364/OE.19.009607